Manganiferous minerals of the epidote group from the Archaean basement of West Greenland

ANNA KATERINOPOULOU, TONCI BALIC-ZUNIC, JOCHEN KOLB, ALFONS BERGER
& KARSTEN SECHER

The chemical compositions and crystal structures of Mn^{3+}-containing minerals from the epidote group in Greenland rocks are investigated and described in detail. They occur in hydrothermally altered Archaean mafic sequences within the gneissic complex of the North Atlantic craton of West Greenland. The Mn-containing minerals have a characteristic red to pink colour. A detailed microchemical study shows a significant inter- and intra-sample variation in Mn content. The samples from different parageneses can be classified as Mn-bearing epidote and Mn-bearing clinozoisite. The intra-sample variation in the content of Al, Fe and Mn is on a very fine scale, but still allows for identification of a negative correlation between Mn and Fe. Textures indicate different stages of growth. Crystal chemical data are compared with literature data and illustrate the basic systematic differences between the influence of Fe and Mn on the crystal structure of the epidote group minerals.

Keywords: Epidote, clinozoisite, Greenland, manganiferous minerals.

A. Katerinopoulou [annak@snm.ku.dk], Natural History Museum of Denmark, Øster Voldgade 5–7, DK-1350 Copenhagen K, Denmark; current address: [akat@topsoe.dk], Haldor Topsøe, Nymøllevej 55, DK-2800 Kgs. Lyngby, Denmark. T. Balic-Zunic [toncib@snm.ku.dk], Natural History Museum of Denmark, Øster Voldgade 5–7, DK-1350 Copenhagen K, Denmark. J. Kolb [jkol@geus.dk] and K. Secher [kse@geus.dk], Geological Survey of Denmark and Greenland (GEUS), Øster Voldgade 10, DK-1350 Copenhagen K, Denmark. A. Berger [ab@geo.ku.dk], Department of Geography and Geology, University of Copenhagen, Øster Voldgade 10, DK-1350 Copenhagen K, Denmark; current address: [alfons.berger@geo.unibe.ch], Institute of Geological Sciences, University of Bern, Switzerland.

Observations of Mn-containing minerals in Greenland have been scarce. Apart from a dubious determination in 1901 by Flink (Bøggild 1953, remark on p. 140) of rhodocrosite within the Proterozoic late Gardar alkaline Narssarsuk pegmatite, Thomassen & Krebs (2001) report manganiferous carbonate in East Greenland, associated with epithermal vein fillings related to the Palaeogene subvolcanic Flammefjeld intrusive complex. These carbonates are the only previously published observations. However, there have been some unpublished reports of pink-coloured minerals from Greenland tentatively described as "thulite", a pink Mn^{2+}-bearing variety of zoisite (O.V. Petersen, personal communication). Here we attempted to analyze in detail all of the known occurrences of the latter type of minerals from Greenland and provide their first full characterization. They all originate from Archean rocks.

Origin of the material and geological setting

The samples carrying manganiferous minerals were collected from three different locations in the areas of Maniitsoq, Tasiusarsuaq and Paamiut, West Greenland (Table 1, Fig. 1). All three areas lie within the Archaean North Atlantic craton which is mainly composed of grey gneisses and narrow belts of supracrustal rocks. The areas mainly comprise amphibolite and mafic granulite, as well as minor metasedimentary and ultramafic rocks (e.g. Windley & Garde 2009). Late-tectonic granitic intrusions are volumetrically minor (e.g.Windley & Garde 2009). The rocks underwent several stages of high-grade metamorphism in granulite and amphibolite facies and several stages of deformation during the Archaean (Friend & Nutman 2001). A mafic dyke swarm intruded the craton in the

Table 1. Origin and characteristics of samples

Sample	Location	Coordinates	Host rock	Manganiferous mineral
492571	Maniitsoq area	65°18.36'N, 51°35.70'W	Pegmatitic/aplitic granulite	Light pink Mn-containing clinozoisite
508347	Tasiusarsuaq terrane	63°56.46'N, 50°03.84'W	Amphibolite (meta-peridotite)	Purple Mn-rich epidote
177975	Paamiut area	62°00.78'N, 49°40.26'W	Amphibolite	Purple Mn-rich clinozoisite*

*Earlier described as 'thulite'

Proterozoic with NW–SE, E–W, and NE–SW orientations (Kalsbeek & Taylor 1985). The dykes intersect mutually and are themselves intersected by kilometre-scale faults and fault zones which are interpreted to be Proterozoic, based on intersection relationships (e.g. Smith & Dymek 1983).

The brittle to brittle–ductile faults are near-vertical and trend N–S, NW–SE, and W–E. They have a lateral displacement of marker horizons of up to 1 km. All faults show a halo of hydrothermal alteration, which for the larger faults may extend to several hundreds of metres (Kolb *et al.* 2009). The hydrothermal alteration is characterized by the greenschist facies assemblage of chlorite, epidote, muscovite and calcite (Kolb *et al.* 2009).
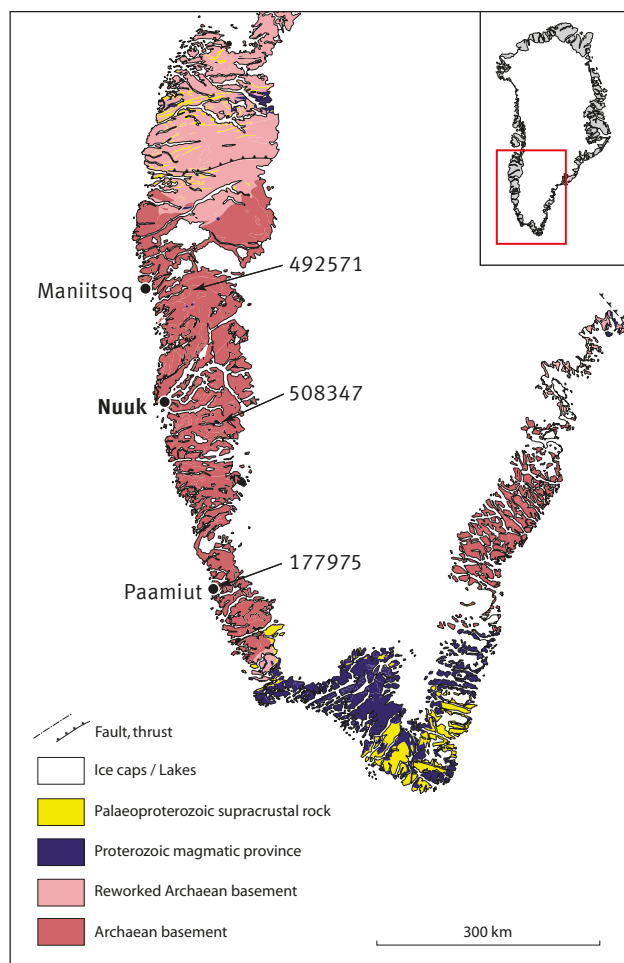

Fig. 1. Map of West Greenland showing the locations of the Mn-bearing mineral samples.

The hydrothermal alteration assemblage locally comprises pyrite and chalcopyrite. The sulphides are commonly oxidized and leached, as witnessed by the formation of hematite, bornite and covellite, which may be related to a later hydrothermal meteoric overprint. The occurrence of the manganiferous minerals analyzed here is restricted to hydrothermal alteration of fault zones in different host rocks.

Sample 492571 represents migmatitic gneiss from the Maniitsoq area. The gneisses have a granulite facies mineral assemblage of orthopyroxene + clinopyroxene + plagioclase + quartz ± magnetite, ilmentite, amphibole and biotite (Riciputi *et al.* 1990). Peak metamorphic conditions are estimated at 800 ± 50°C and 7.9 ± 1 kbar (Riciputi *et al.* 1990). Retrogression in amphibolite facies is widespread, whereas a greenschist facies overprint is restricted to fault zones (Riciputi *et al.* 1990; Windley & Garde 2009).

Sample 508347 represents a meta-ultramafic dyke or sill from the Tasiusarsuaq terrane (Kolb *et al.* 2012). Three rock types are distinguished in the locality: (1) a massive, medium-grained greenish to brownish weathering rock with a clinopyroxene + hornblende + orthopyroxene + magnetite ± garnet ± biotite ± olivine ± calcite ± cummingtonite ± pyrrhotite ± chalcopyrite assemblage; (2) a layered, medium-grained grey rock with centimetre-scale black hornblende ± quartz ± titanite ± calcite ± magnetite layers and grey hornblende + plagioclase layers; (3) a massive, medium-grained, black rock consisting of hornblende + clinopyroxene + orthopyroxene + pyrrhotite + magnetite. They represent meta-pyroxenites and meta-peridotites that were overprinted at 7–12 kbar and 750–840°C (Riciputi *et al.* 1990; Wells 1976). Retrograde amphibolite facies conditions are estimated at 7 kbar and 630°C (Riciputi *et al.* 1990; Wells 1976). A dilational jog south of Ameralik fjord is a few hundred metres wide and intensely altered and mineralized by a stockwork quartz vein system containing up to 25 ppm Ag and 2 wt% Cu (Appel *et al.* 2005; Kolb *et al.* 2009). The hydrothermal system is interpreted to be controlled by deformation along the faults. Focusing of fluids and stockwork-type veining and mineralization is controlled by regional anisotropies represented in this case by the dilational jog. Greenschist facies assemblages close to the fault zones comprise epidote + chlorite + quartz + serpentine + talc ± rutile ± titanite.

Sample 177975 from the Paamiut area is a chip from a large ice-transported boulder of more than 200 kg. This impressive piece of purple coloured float has never been unambiguously traced to an in-situ locality, although it probably originates from similar rocks containing purple epidote-like minerals that have been observed in the eastern part of the Paamiut area (F. Kalsbeek, personal communication). It is an amphibolite with a characteristic assemblage comprising hornblende + plagioclase + quartz ± garnet and minor titanite, magnetite, ilmenite and apatite. The boulder from which the sample was taken shows stockwork vein sets and a greenschist facies alteration assemblage of clinozoisite/epidote + albite + quartz.

Experimental

Mineral chemical analyses were performed on polished thin sections using a JEOL JXA8200 electron microprobe (EMP) located at the Department of Geography and Geology of the University of Copenhagen. Measuring conditions were 15 kV and 15 nA, all elements were measured with WDS using natural and synthetic oxides and silicates as standards. Corrections of the raw data were performed using the ZAF procedure.

Single crystals of reddish to pink colour were optically hand-picked from the rock samples for X-ray diffraction (XRD). Analyses were performed using a Bruker-AXS four-circle diffractometer equipped with a CCD area detector and a flat graphite monochromator, using MoKα radiation from a fine-focus sealed X-ray tube. A total of 2800 exposures per sample (step = 0.2°, time/step = 10 s) covering the full reciprocal sphere were collected. Data collection, intensity integration and absorption correction were carried out with the Bruker programs Smart, Saint and Sadabs respectively. After space group identification the structure was refined using the structure model of Dollase (1971) as starting model. Occupancies were refined and the mean electron number was used to elaborate on the composition of the samples. For sites A1 and A2 the number of electrons was 20 within standard deviation, and site populations were fixed to full Ca occupation. Refinement data are reported in Table 2.

Table 2. Refinement details for the three samples

Sample number	492571	508347	177975
Empirical formula (XRD+EMPA)*	$Ca_2Al_{2.78}Fe_{0.21}Mn_{0.02}Si_3O_{12}(OH)$	$Ca_2Al_{2.20}Fe_{0.60}Mn_{0.13}Si_3O_{12}(OH)$	$Ca_2Al_{2.51}Fe_{0.47}Mn_{0.02}Si_3O_{12}(OH)$
Formula weight M_r	965.6	884.7	966.5
Crystal System	monoclinic	monoclinic	monoclinic
Z	2	2	2
F(000)	477	438	478
$\mu(mm^{-1})$	3.36	3.18	3.44
$\varrho\chi$ (gr cm^{-3})	3.52	3.20	3.51
Space group (no.)	P2(1)/m (11)	P2(1)/m (11)	P2(1)/m (11)
a (Å)	8.8790(9)	8.8891(5)	8.8890(7)
b (Å)	5.5947(1)	5.6255(3)	5.6149(5)
c (Å)	10.1570(9)	10.1605(5)	10.1601(8)
β (°)	115.483(6)	115.447(1)	115.439(2)
V (Å^3)	455.47	458.79	457.93
Number of reflections/Unique	4769/1463 (R_{int} = 0.0498)	4926/1525 (R_{int} = 0.0304)	5060/1524 (R_{int} = 0.0511)
Data/restraints/parameters	1463/0/119	1525/0/119	1524/0/119
Extinction coefficient k	0	0	0
Goodness-of-fit, S	0.807	0.767	0.824
R indices for I>2σ(I)	R_1 = 0.0355	R_1 = 0.0208	R_1 = 0.0390
R indices (all data)	R_1 = 0.0531	R_1 = 0.0225	R_1 = 0.0608
	wR_2 = 0.1131	wR_2 = 0.0861	wR_2 = 0.1256

$R_1 = \sum ||Fo|-|Fc|| / \sum |Fo|$

$wR_2 = [\sum[w(Fo^2-Fc^2)^2] / \sum[w(Fo^2)^2]]^{0.5}$

*The proportions of Al, Fe and Mn are calculated on the basis of the m.e.n. (Table 4) by taking into account the Fe:Mn ratio calculated from the EMPA results (Table 3).

Table 3. Chemical compositions of epidote-group minerals.

Sample	492571			492571		
	High Fe			Low Fe		
	N=3			N=7		
	wt%	stdev	Range	wt%	stdev	Range
Al_2O_3	28.52	0.33	28.15 - 28.77	31.41	0.42	30.62 - 31.88
Fe_2O_3	5.76	0.31	5.50 - 6.10	2.20	0.28	1.92 - 2.70
CaO	23.86	0.20	0.01 - 0.02	24.50	0.37	24.05 - 25.01
MgO	0.02	0.01	0.01 - 0.02	0.11	0.03	0.05 - 0.16
SiO_2	39.01	0.33	0.00 - 0.21	39.39	0.35	38.78 - 39.80
Mn_2O_3	0.08	0.11	0.00 - 0.21	0.30	0.09	0.18 - 0.41
TiO_2	0.02	0.03	0.00 - 0.06	0.16	0.11	0.02 - 0.27
Total	97.27	0.91	96.24 - 97.96	98.07	0.88	96.63 - 99.24
Recalculation to cations on the basis of O = 12.5						
Al	2.64	0.01	2.64 - 2.65	2.84	0.02	2.82 - 2.85
Fe	0.38	0.02	0.36 - 0.40	0.14	0.02	0.12 - 0.18
Ti	0.00	0.00	0.00 - 0.00	0.01	0.01	0.00 - 0.02
Si	3.07	0.00	3.06 - 3.07	3.02	0.01	3.01 - 3.04
Mn	0.01	0.01	0.00 - 0.01	0.02	0.01	0.01 - 0.03
Ca	2.01	0.02	1.99 - 2.02	2.01	0.01	1.99 - 2.03
Mg	0.00	0.00	0.00 - 0.00	0.01	0.00	0.01 - 0.02
Total	8.11	0.00	0.00 - 8.11	8.05	0.01	8.04 - 8.06

Analyses of sample 492571 are categorized according to the Fe content

Sample	508347			177975		
	N=49			N=33		
	wt%	std dev	Range	wt%	std dev	Range
Al_2O_3	23.68	0.92	21.58 - 25.39	28.47	2.08	25.31 - 31.47
Fe_2O_3	11.74	2.07	8.33 - 15.55	4.53	3.24	1.00 - 11.06
TiO_2	0.05	0.05	0.00 - 0.22	0.06	0.06	0.00 - 0.21
Na_2O	0.01	0.01	0.00 - 0.04	0.02	0.05	0.00 - 0.28
SiO_2	37.67	0.29	36.96 - 38.19	38.34	0.59	37.40 - 39.47
Mn_2O_3	1.30	1.06	0.00 - 3.56	1.35	1.72	0.02 - 5.89
CaO	23.93	0.23	23.42 - 24.33	24.58	0.43	23.85 - 25.31
MgO	0.03	0.03	0.00 - 0.09	0.06	0.05	0.00 - 0.17
$Cr2O_3$	0.02	0.02	0.00 - 0.08	0.01	0.02	0.00 - 0.06
Total	98.43	0.61	96.91 - 99.57	97.43	0.73	96.15 - 99.38
Recalculation to cations on the basis of O = 12.5						
Al	2.21	0.08	2.02 - 2.34	2.62	0.17	2.34 - 2.85
Fe	0.70	0.12	0.50 - 0.93	0.27	0.19	0.06 - 0.65
Ti	0.00	0.00	0.00 - 0.01	0.00	0.00	0.00 - 0.01
Na	0.00	0.00	0.00 - 0.01	0.00	0.01	0.00 - 0.04
Si	2.99	0.01	2.95 - 3.01	2.99	0.02	2.95 - 3.03
Mn	0.08	0.06	0.00 - 0.22	0.08	0.10	0.00 - 0.35
Ca	2.03	0.02	1.98 - 2.08	2.05	0.02	2.01 - 2.10
Mg	0.00	0.00	0.00 - 0.01	0.01	0.01	0.00 - 0.02
Cr	0.00	0.00	0.00 - 0.00	0.00	0.00	0.00 - 0.00
Total	8.02	0.01	8.00 - 8.04	8.02	0.01	8.00 - 8.06

Results

Chemical compositions and mineral associations

The results of the microprobe analyses of the pink coloured minerals from the three investigated samples are presented in Table 3. X-ray diffraction results show that they all belong to the epidote group of minerals which is in accordance with their chemical composition. The measured variation of the Al→Fe,Mn substitution in sample 177975 indicates a continuous solid solution (Fig. 2), whereas this variation in sample 492571 lacks compositions within the proposed immiscibility gap of the clinozoisite-epidote series around 25% epidote (Raith 1976; Heuss-Aßbichler & Fehr 1997). Sample 508347 lies on the high-Fe side of the proposed immiscibility gap and is thus not indicative (Fig. 2).

The mineral assemblage determined by EMP analysis in sample 492571 (migmatitic gneiss from Maniitsoq) characterizes the greenschist facies and comprises coexisting clinozoisite and quartz, tremolite, titanite and zircon (Fig. 3a). Clinozoisite appears in masses of irregular grains, which consist of iron-rich rims (approx. 0.40 Fe apfu) and iron-poor cores (approx. 0.12 Fe apfu) (Fig. 3b). The cores are sometimes more complex with an euhedral zone with an intermediate (Fe+Mn)/Al ratio surrounded by an irregular second zone that is characterized by low (Fe+Mn)/Al

ratio (Zones I and II, respectively on Fig. 3b). Fe-rich rims follow the grain boundaries or make lobate intrusions in the cores (Zone III on Fig. 3b). The appearance of zone III indicates a post-crystallization replacement process by a fluid richer in Fe. The apparent compositional gap is thus most probably due to this secondary enrichment in Fe which ceased at some time without subsequent homogenization of clinozoisite.

In sample 508347 (meta-peridotite), two textural types of epidote are observed: (1) euhedral grains ~100μm in size (Fig. 4a) and (2) massive aggregates of anhedral grains (Fig. 4b). These textural types do not have any distinctive compositional differences. Epidote shows variable amounts of Mn and Fe (Fig. 2). Compositions of the grains cover a broad range, extending from high Fe, low Mn and reaching close to the epidote-clinozoisite boundary with a wide scope

Fig. 3. Back-scattered electron images of sample 492571 (from felsic migmatitic gneiss). **A**: Clinozoisite in association with quartz and minor tremolite. **B**: Close-up of the clinozoisite assemblage with compositional zoning indicated, as described in the text.
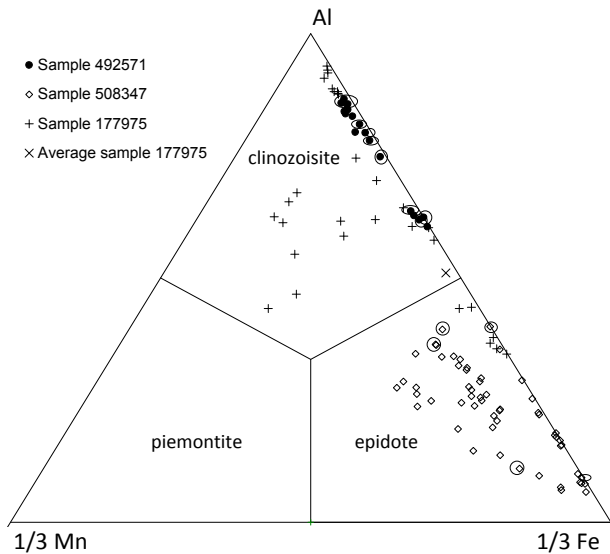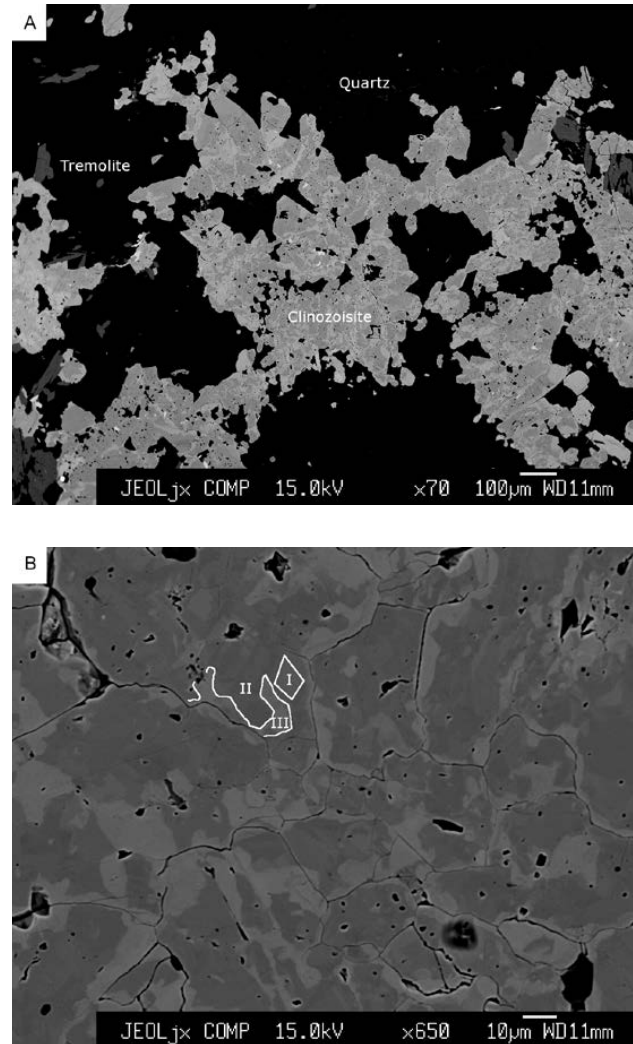

Fig. 2. Ternary diagram (Al–Mn–Fe) showing the octahedral cation population of epidote group minerals calculated from the results of microprobe analysis. Ellipses surround the compositions found for the 492571 and 508347 crystals investigated by XRD. The average composition of the crystal from 177975 is inferred from XRD results assuming 0.02 wt% Mn.

of Mn content reaching up to 0.22 apfu. The enrichment in Mn is variable on a small scale and is generally negatively correlated with the Fe content. Several points with almost no Mn extend broadly along the epidote-clinozoisite join. It seems that the local variations in Mn during the growth of epidote caused a high degree of compositional inhomogeneity. One possible explanation is that the Mn content originates from the metamorphosed rock and depended on the distribution of primary Mn-containing minerals and their transformation paths.

In sample 177975 (amphibolite), the hydrothermal veins exhibit (1) clinozoisite selvages with 0.01–0.07 Fe apfu; (2) a fine-grained zone of mixed clinozoisite and epidote; (3) a broader zone dominated by larger crystals of subhedral Fe-rich clinozoisite (Fig. 5). There

is a strong variation in the Mn-Fe content, sometimes even within the same crystal. The zonation is also optically detectable in the variable colour of the hand specimen. The content of Mn^{3+}, which is responsible for the red colour, has a range of 0-0.35 apfu in the sample (Fig. 2). This sample has on average the highest Mn-content of all the investigated samples.

It is interesting that the points with the lowest and highest Fe-contents show very small amounts of Mn, whereas those with intermediate compositions (corresponding to Fe-rich clinozoisite) show a large variation and sometimes significant enrichment in Mn (Fig. 2). Some parts are relatively enriched in manganese and reach the boundaries of the piemontite field. This enrichment occurs on a small scale and these crystals are in direct contact with Mn-poor areas. This illustrates the fact that even small amounts of Mn^{3+} are enough to give pink colouring, even in the presence of a high iron content.

Considering the large variations in compositions of clinozoisite and epidote in all three samples, the three crystals chosen for the crystal structure analysis were prepared for EMP analysis after the XRD measurement. Unfortunately, the crystal from 177975 was lost during the polishing process and its composition can only be reconstructed on the basis of its crystal structure. This shows that it has roughly average composition close to the clinozoisite-epidote boundary with a low Mn content (Fig. 2 and Table 2). The crystal from 492571 has an average composition of $Ca_2Al_{2.78}Fe_{0.21}Mn_{0.02}Si_3O_{12}(OH)$ determined from eight spot measurements with a relatively high variation in Al:Fe ratio from 62:37 to 81:12, encompassing
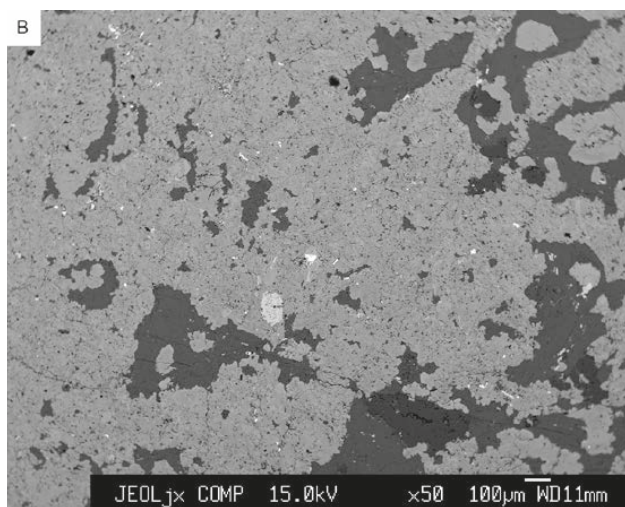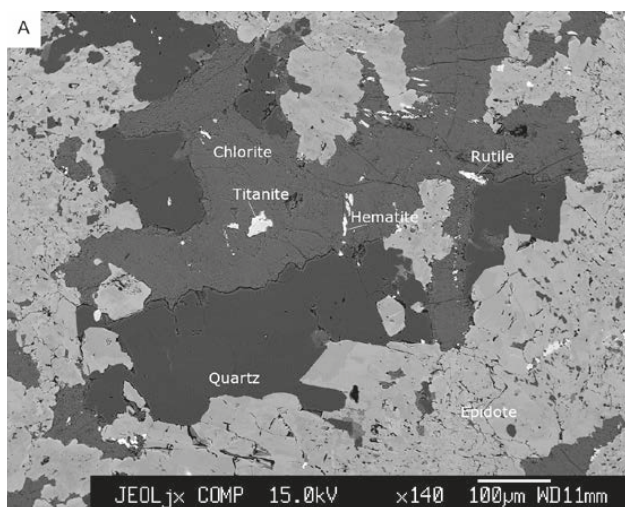

Fig. 4. Back-scattered electron images of sample 508347 (metaperidotite). **A**: Euhedral grains of epidote ranging into anhedral massive epidote in association with chlorite, quartz and accessory titanite and rutile. **B**: Massive anhedral epidote with interdispersed chlorite and minor quartz.
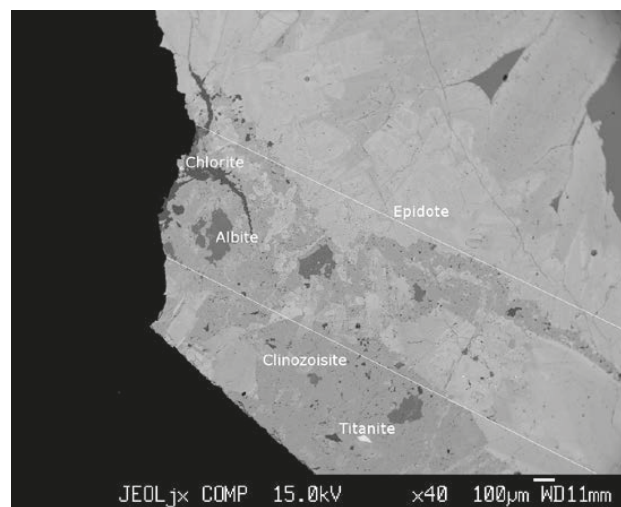

Fig. 5. Back-scattered electron image of sample 177975 (amphibolite). Lines are used as a guide to the eye to indicate the different zones within the sample.

Table 4. Atomic parameters and equivalent isotropic thermal factors U_{eq} for the three investigated samples

sample	492571	508347	177975	sample	492571	508347	177975
A1 (Ca)				z	0.0451(2)	0.04137(12)	0.0433(3)
x	0.76082(11)	0.75837(6)	0.75933(12)	U	0.0110(4)	0.0092(2)	0.0083(5)
y	0.75	0.75	0.75	O2			
z	0.15481(9)	0.15276(5)	0.15336(11)	x	0.3010(2)	0.30284(14)	0.3021(3)
U	0.0120(2)	0.01080(13)	0.0087(3)	y	0.9859(4)	0.98298(18)	0.9839(4)
A2 (Ca)				z	0.3521(2)	0.35456(11)	0.3535(3)
x	0.60639(11)	0.60516(6)	0.60581(12)	U	0.0110(4)	0.0096(2)	0.0089(5)
y	0.75	0.75	0.75	O3			
z	0.42342(9)	0.42398(5)	0.42368(11)	x	0.7890(3)	0.79268(14)	0.7912(3)
U	0.0135(2)	0.01331(14)	0.0109(3)	y	0.0129(4)	0.01352(18)	0.0138(4)
occ	Ca	Ca	Ca	z	0.3454(2)	0.34160(11)	0.3430(3)
M1 (Al)				U	0.0118(4)	0.0106(2)	0.0098(5)
x	0	0	0	O4			
y	0	0	0	x	0.0550(4)	0.0536(2)	0.0538(4)
z	0	0	0	y	0.25	0.25	0.25
U	0.0081(3)	0.00652(15)	0.0028(5)	z	0.1315(3)	0.13002(16)	0.1299(4)
occ	Al	Al	Al	U	0.0080(5)	0.0075(3)	0.0050(6)
M2 (Al)				O5			
x	0	0	0	x	0.0389(3)	0.04113(19)	0.0398(4)
y	0	0	0	y	0.75	0.75	0.75
z	0.5	0.5	0.5	z	0.1428(3)	0.14476(16)	0.1441(4)
U	0.0079(3)	0.00687(15)	0.0026(5)	U	0.0087(6)	0.0079(3)	0.0075(7)
occ	Al	Al	Al	O6			
M3				x	0.0600(4)	0.06388(19)	0.0629(4)
x	0.28911(13)	0.29235(5)	0.29151(12)	y	0.75	0.75	0.75
y	0.25	0.25	0.25	z	0.4013(3)	0.40444(16)	0.4039(4)
z	0.22408(11)	0.22404(4)	0.22430(11)	U	0.0090(6)	0.0084(3)	0.0062(7)
U	0.0089(3)	0.00713(14)	0.0061(3)	O7			
m.e.n.	15.67(8) [15.47]	20.75(4) [21.77]	19.60(9) [19.35]	x	0.5159(4)	0.5150(2)	0.5147(4)
T1 (Si)				y	0.75	0.75	0.75
x	0.33854(14)	0.33893(7)	0.33907(16)	z	0.1775(3)	0.17991(17)	0.1786(4)
y	0.75	0.75	0.75	U	0.0121(6)	0.0106(3)	0.0110(7)
z	0.04803(12)	0.04733(6)	0.04775(15)	O8			
U	0.0081(2)	0.00638(14)	0.0054(3)	x	0.5118(4)	0.5212(2)	0.5187(4)
T2 (Si)				y	0.25	0.25	0.25
x	0.67930(14)	0.68243(7)	0.68143(16)	z	0.2969(4)	0.30533(19)	0.3031(5)
y	0.25	0.25	0.25	U	0.0151(6)	0.0148(3)	0.0122(8)
z	0.27523(12)	0.27499(6)	0.27509(15)	O9			
U	0.0080(2)	0.00679(14)	0.0052(3)	x	0.6392(4)	0.6297(2)	0.6340(5)
T3 (Si)				y	0.25	0.25	0.25
x	0.18260(13)	0.18335(7)	0.18333(15)	z	0.1036(3)	0.10006(17)	0.1013(4)
y	0.75	0.75	0.75	U	0.0201(7)	0.0165(3)	0.0155(8)
z	0.31628(12)	0.31780(6)	0.31744(15)	O10			
U	0.0077(2)	0.00622(14)	0.0051(3)	x	0.0758(4)	0.08072(19)	0.0776(4)
O1				y	0.25	0.25	0.25
x	0.2346(3)	0.23341(14)	0.2343(3)	z	0.4234(3)	0.42734(16)	0.4249(4)
y	0.9959(3)	0.99465(17)	0.9946(4)	U	0.0095(6)	0.0083(3)	0.0075(7)

A list of anisotropic thermal factors can be provided by the authors upon request. The occupancy of site M3 is represented by the refined mean electron number (m.e.n.) for this site. The m.e.n. calculated from EMPA is in [] brackets.

almost the entire range found in the large sample and representing both the Fe-poor core and Fe-rich rim. The crystal from 508347 has an average composition of $Ca_2Al_{2.20}Fe_{0.60}Mn_{0.13}Si_3O_{12}(OH)$ from five spot measurements. There is a large compositional variation within the crystal, which is immediately detectable in the backscatter image (Fig. 4). Part of the crystal has a composition with a very low Mn content (0.003 apfu) but a high Fe content, whereas other parts have Mn up to 0.11 apfu. The average composition of the crystal falls practically in the middle of the composition field for the sample (Fig. 2).

Crystallographic data

Single crystal X-ray diffraction of selected crystals confirms the clinozoisite-type structure for all three samples and substitution of Al, Fe and Mn, as expected for this structural family (Table 4). According to the structure refinement, Fe and Mn are exclusively present on the M3 site.

Identification of the proportion of Fe and Mn in the structure is not straightforward from X-ray diffraction data because the scattering factors of Fe and Mn are similar. It is, however, expected that the two have a different effect on the geometrical parameters of the crystal structure because of the Jahn–Teller effect of Mn^{3+} (Langer *et al.* 2002). The $3d^4$-configuration of M^{3+} in octahedral coordination causes splitting of the ^5E_g octahedral crystal-field ground state. The $3d^5$-configured Fe^{3+} behaves differently when incorporated in

the structure and does not deviate from sphericity. The differences between Fe^{3+} and Mn^{3+} might influence the average bond distances and volumes and the distortion parameters of the coordination polyhedra. To explore this effect, we plotted data from crystal structures of synthetic and natural members of the epidote group of minerals (Dollase 1968; Gabe *et al.* 1973; Nozic *et al.* 1978; Stergiou *et al.* 1987; Comodi & Zanazzi 1997; Giuli *et al.* 1999; Nagashima & Akasaka 2004) with different substitution degrees of Fe and Mn. For the calculation of crystal chemical parameters we used the program IVTON (Balic-Zunic & Vickovic 1996).

Looking at the asphericity of the octahedra, i.e. the relative discrepancy of the ligands from the surface of the common sphere (Balic-Zunic & Makovicky 1996), it is clear that the asphericity can be expected to be significantly higher for Mn at the M3 site compared to Fe (Fig. 6a). Similar to the asphericity, the volume-based distortion (Makovicky & Balic-Zunic 1998) of the M3 site is larger for Mn-bearing samples than for Fe-bearing ones (Fig. 6b). Distortion seems to follow a linear trend with variation in chemistry, which changes at 0.6 apfu Fe in the clinozoisite–epidote series and 1 apfu Mn in the clinozoisite–piemontite series, representing the change of substitution mechanism with large Fe or Mn concentrations (Franz & Liebscher 2004). The trends are of decreasing asphericity and increasing volume distortion with increasing Fe or Mn content.
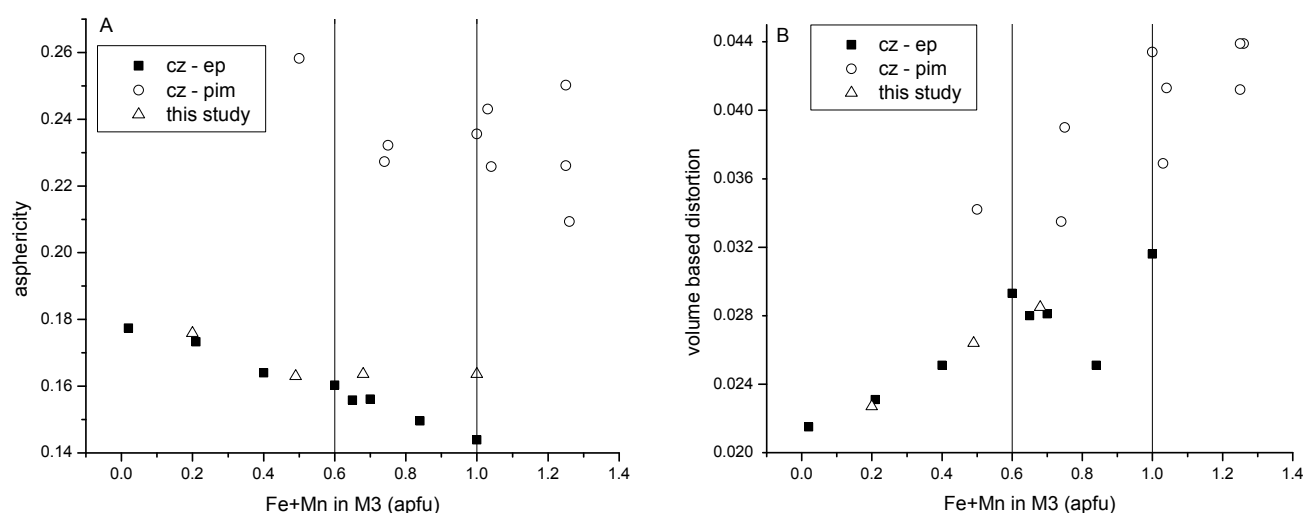
Fig. 6. Distortion parameters of the M3 polyhedron. **A**: Asphericity. **B**: Volume-based distortion. Cz: clinozoisite, ep: epidote, pim: piemontite. Clinozoisite–epidote data from Comodi & Zanazzi (1997), Dollase (1968, 1971), Gabe *et al.* (1973), Giuli *et al.* (1999) and Stergiou *et al.* (1987). Clinozoisite–piemontite data from Dollase (1969) and Nagashima & Akasaka (2004). Lines at 0.6 and 1 apfu mark the change in substitution mechanism for Fe and Mn, respectively.

Discussion

The crystal structure of the epidote group minerals with the general formula A1A2M1M2M3T$_3$O$_{12}$(OH) contains three types of octahedral sites: M1, M2 and M3. M1 octahedra share edges and form chains that run along the b axis. Individual M3 octahedra are attached to these chains on alternate sides, thus forming a zig-zag M1/M3 octahedral chain. M2 octahedra share edges and form separate simple chains that also run parallel to the b axis. The two types of octahedral chains are bridged by SiO$_4$ tetrahedra and Si$_2$O$_7$ groups (T in the general formula stands for the tetrahedral cation, in this case Si). In the spaces between the octahedral chains there are two crystallographically distinct sites, A1 and A2 coordinated by 9 and 10 oxygens, respectively. A-type sites are mainly occupied by Ca. The trivalent cations such as Al, Mn^{3+} and Fe^{3+} are distributed over the octahedral M sites. The classification rules for the solid solution series in the clinozoisite subgroup, where Ca occupies the A site, are based on the observation that the atomic substitutions take place predominately on the M3 sites. The M1 site accommodates some Fe and Mn only in samples with very high contents of these elements, whereas M2 remains practically a pure Al site. In accordance with this, the compositions which have a predominating content of Al in the M3 site are called clinozoisite, those with most Fe at this site are called epidote, and those that have Mn as the dominating cation are called piemontite (Armbruster *et al.* 2006). The M3 octahedron is located on the mirror plane. It is the largest and most distorted octahedron in the structure.

Unlike M1 and M2 coordination octahedra, which form infinite chains by trans-edge sharing, the M3 polyhedron is only side-attached to the (M1) chain. This leaves a possibility to fill this site with a cation larger than Al. The bond distances and volume of the M3 polyhedron increase by rotation of the silicate tetrahedra with which the M3 polyhedron shares corners without influencing significantly the size of the M1 and M2 octahedral chains.

The incorporation of ions larger than Al in this site is therefore preferable. According to Bonazzi & Menchetti (1995) and Franz & Liebscher (2004), the volume of M3 increases with increasing Fe content, accompanied by the rotation of T1O$_4$ and T2O$_4$ tetrahedra with decreasing T1-O9-T2 angle. Nagashima & Akasaka (2004) observed the same structure changes with increasing Mn^{3+} content.

The substitution mechanism has been previously studied in natural and synthetic solid solutions along the clinozoisite-epidote join (Belov & Rumanova 1953, 1954; Ito *et al.* 1954; Dollase 1968, 1971; Gabe *et al.* 1973; Nozic *et al.* 1978; Stergiou *et al.* 1987; Comodi & Zanazzi 1997; Giuli *et al.* 1999; Langer *et al.* 2002) and the clinozoisite-piemontite join (Dollase 1969; Bonazzi & Menchetti 2004; Nagashima & Akasaka 2004, 2010). A change in substitution mechanism in these solid solutions at about 0.6 Fe pfu or 1 Mn pfu, respectively, has been suggested by Franz & Liebscher (2004). At concentrations higher than these, Fe or Mn are suggested to begin to enter the M1 site. It has also been proposed that small amounts of Fe^{2+} or Mn^{2+} can enter the A-sites in the clinozoisite sub-group (Bonazzi & Menchetti 2004; Nagashima & Akasaka 2010). There were no such indications from our X-ray diffraction data, in accordance with the results of the chemical analysis.

As regards the parameters of the M3 coordination polyhedron, only sample 508347 shows deviation from the pure clinozoisite-epidote trend and indication of the Mn content (Fig. 7). It is interesting that the distortion parameters do not indicate the point where the content of Mn seems to be insufficient to produce a significant deviation, whereas this is clearly visible in the bond lengths and size of the coordination polyhedra. Sample 492571 has only 1–2 mol% of Mn and it is not surprising that its influence cannot be observed. For sample 177975 we can conclude that the amount of Mn does not exceed a few mol% according to its crystal chemical parameters, but it is still sufficient to give the crystal its characteristic pink colour. Considering the large variation of the Mn content in this sample
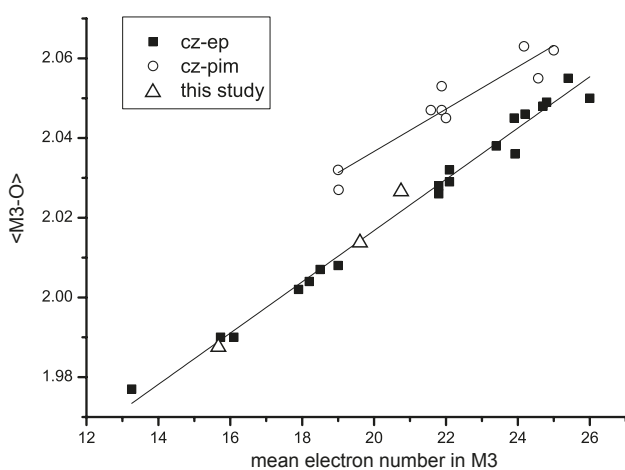
Fig. 7. Mean bond distance plotted against mean electron number for the M3 site. Cz: clinozoisite, ep: epidote, pim: piemontite. Clinozoisite–epidote data from Bonazzi & Menchetti (1995), Comodi & Zanazzi (1997), Dollase (1968, 1971), Gabe *et al.* (1973), Giuli *et al.* (1999), Langer *et al.* (2002) and Stergiou *et al.* (1987). Clinozoisite–piemontite data from Dollase (1969 and Nagashima & Akasaka 2004). Regression lines were fitted with a linear least squares function for each solid solution series.

and due to the fact that the amount of Mn in the single crystal could not be experimentally determined, the Mn content ascribed to the crystal in Table 2 should be considered tentative.

The occurrence of the Mn-bearing minerals is related to vein formation within the West Greenland basement and the petrological implications point to a more widespread Mn- source introduced during the cratonic stages of Archaean Greenland.

There is a considerable variation in chemistry and texture of the manganiferous minerals described in this study. We could confirm by single-crystal X-ray diffraction and chemical analysis that they all belong to the epidote group of minerals and include both epidote and clinozoisite members enriched in Mn to varying degrees. The Mn content in the three analyzed samples varies significantly, although all of them have a similar appearance with a characteristic pink to purple colour. The mineral in the retrograde altered migmatitic gneiss (492571) is clinozoisite with a small amount of Mn (1 to 2 mol% in M3 site) which exhibits incomplete replacement of an original Fe-poor clinozoisite by a Fe-enriched variety in the last hydrothermal stage. The sample from the amphibolized meta-peridotite (508347) is epidote with a pronounced negative correlation in the content of Mn and Fe (Fig. 2). The sample from amphibolite (177975) locally shows the highest concentration of Mn of all three investigated samples and lies predominantly in the clinozoisite field, although the Fe-richest domains reach the epidote field. It is interesting that the medium-Fe portions of the sample typically show the highest Mn contents. A somewhat less clear negative correlation between Mn and Fe contents is observed in this sample (Fig. 2). However, the trends are difficult to define because the variation in content of Al, Fe and Mn is extensive and on a very fine scale. According to textural observations Mn has been mobilized in several stages, appearing both in larger euhedral grains and in fine grained anhedral material. The two textural types of epidote are similar in terms of Mn, Fe and Al variations, sometimes within the same crystal. They occur in veins produced by hydrothermal processes and their composition seems to depend strongly both on fluid composition and on the original chemical composition of the altered minerals.

The crystal chemical data available for the epidote group of minerals show discrepancies between synthetic and natural samples which can be attributed to the influence of quenching of the synthetic ones (Giuli *et al.* 1999). There is also a general lack of data from the natural samples with well documented chemical composition and crystal structure, especially for Mn-containing members of the group. Although this impedes the conclusion about the Mn/Fe ratios from

the crystal structure analysis, we could document for the epidote sample the influence of around 10 mol% Mn on the crystal chemical parameters of the M3 site. Taking into account the speed of acquisition and accuracy of the new generation of single crystal diffractometers, we see this as an encouragement to use single-crystal diffraction in combination with chemical analysis for a routine, full characterisation of minerals from the epidote group. Our results show that minerals from this group achieve and retain a substantial chemical inhomogeneity without losing the structural homogeneity.

Acknowledgements

References

Appel, P.W.U., Coller, D., Coller, V., Heijlen, W., Moberg, E.D., Polat, A., Raith, J., Schjødt, F., Stendal, H. & Thomassen, B. 2005: Is there a gold province in the Nuuk region? Report from field work carried out in 2004. Rapport Danmarks og Grønlands Geologiske Undersøgelse 2005/27, 79 pp.

Armbruster, T., Bonazzi, P., Akasaka, M., Bermanec, V., Chopin, C., Gieré, R., Heuss-Assbichler, S., Liebscher, A., Menchetti, S., Pan, Y. & Pasero, M. 2006: Recommended nomenclature of epidote-group minerals. European Journal of Mineralogy 18 (5), 551–567.

Balic-Zunic, T. & Makovicky, E. 1996: Determination of the centroid or "the best centre" of a coordination polyhedron. Acta Crystallographica B52, 78–81.

Balic-Zunic, T. & Vickovic, I. 1996: IVTON - Program for the calculation of geometrical aspects of crystal structures and some crystal chemical applications. Journal of Applied Crystallography 29, 305–306.

Belov, N.V. & Rumanova, I.M. 1953: The crystal structure of epidote $Ca_2Al_2FeSi_3O_{12}(OH)$. Doklady Akademii Nauk SSSR 89, 853–856.

Belov, N.V. & Rumanova, I.M. 1954: The crystal sructure of epidote. Trudy Instituta Kristallografii, Akademiya Nauk SSSR 9, 103–163.

Bøggild, O.B. 1953: The mineralogy of Greenland. Meddelelser om Grønland 149 (3), 442 only.

Bonazzi, P. & Menchetti, S. 1995: Monoclinic members of the epidote group: effects of the Al–Fe^{3+}–Fe^{2+} substitution and of the entry of REE^{3+}. Mineralogy and Petrology 53, 133–153.

Bonazzi, P. & Menchetti, S. 2004: Manganese in monoclinic members of the epidote group: piemontite and related minerals. Reviews in Mineralogy and Geochemistry 56, 495–552.

Comodi, P. & Zanazzi, F. 1997: The pressure behavior of clinozoisite and zoisite: An X-ray diffraction study. American Mineralogist 82, 61–68.

Dollase W.A. 1968: Refinement and comparison of the structures of zoisite and clinozoisite. American Mineralogist 53, 1882–1898.

Dollase W.A. 1969: Crystal structure and cation ordering of piemontite. American Mineralogist 54, 710–717.

Dollase W.A. 1971: Refinement of the crystal structures of epidote, allanite and hancockite. American Mineralogist 56, 447–464.

Franz, G. & Liebscher, A. 2004: Physical and chemical properties of the epidote minerals–An introduction. Reviews in Mineralogy and Geochemistry 56, 1–80.

Friend, C.R.L. & Nutman, A.P. 2001: U-Pb zircon study of tectonically bounded blocks of 2940–2840 Ma crust with different metamorphic histories, Paamiut region, South-West Greenland: implications for the tectonic assembly of the North Atlantic craton. Precambrian Research 105 (2–4), 143–164.

Gabe, E.J., Portheine, J.C. & Whitlow, S.H. 1973: A reinvestigation of the epidote structure: Confirmation of the iron location. American Mineralogist 58, 218–223.

Giuli, G., Bonazzi, P. & Menchetti, S. 1999: Al–Fe disorder in synthetic epidotes: A single-crystal X-ray diffraction study. American Mineralogist 84, 933–936.

Heuss-Aßbichler, S. & Fehr, K.T. 1997: Intercrystalline exchange of A1 and Fe^{3+} between grossular–andradite and clinozoisite–epidote solid solutions. Neues Jahrbuch für Mineralogie, Abhandlungen 172 (1), 69–100.

Ito, T, Morimoto, N. & Sadanaga, R. 1954: On the structure of epidote. Acta Crystallographica 7, 53–59.

Kalsbeek, F. & Taylor, P. 1985: Age and origin of early Proterozoic dolerite dykes in South-West Greenland. Contributions to Mineralogy and Petrology 89 (4), 307–316.

Kolb, J., Stensgaard, B.M., Schlatter, D.M. & Dziggel, A. 2009: Controls of hydrothermal quartz vein mineralisation and wall rock alteration between Ameralik and Sermilik, southern West Greenland. Rapport Danmarks og Grønlands Geologiske Undersøgelse 2009/25, 76 pp.

Kolb, J., Kokfelt, T. & Dziggel, A. 2012: Deformation history of an Archaean terrane at mid-crustal level: the Tasiusarsuaq terrane of southern West Greenland. Precambrian Research 212–213, 34–56.

Langer, K., Tillmanns, E., Kersten, M., Almen, H. & Arni, R.K. 2002: The crystal chemistry of Mn^{3+} in the clino- and orthozoisite structure types, $Ca_2M^{3+}_3[OH/O/SiO_4/Si_2O_7]$: A structural and spectroscopic study of some natural piemontites and "thulites" and their synthetic equivalents. Zeitschrift für Kristallographie 217, 563–580.

Makovicky E. & Balic-Zunic, T. 1998: New measure of distortion for coordination polyhedra. Acta Crystallographica B54, 766–773.

Nagashima, M. & Akasaka, M. 2004: An X-ray Rietveld study of piemontite on the join $Ca_2Al_3Si_3O_{12}(OH)$–$Ca_2Mn_3^{3+}Si_3O_{12}(OH)$ formed by hydrothermal synthesis. American Mineralogist 89, 1119–1129.

Nagashima, M. & Akasaka, M. 2010: X-ray Rietveld and [57]Fe Mössbauer studies of epidote and piemontite on the join $Ca_2Al_2Fe^{3+}Si_3O_{12}(OH)$–$Ca_2Al_2Mn^{3+}Si_3O_{12}(OH)$ formed by hydrothermal synthesis. American Mineralogist 95, 1237–1246.

Nozic, Y.Z., Kanepit, V.N., Fykin, L.Y. & Makarov, Yu.S. 1978: A neutron-diffraction study of the structure of epidote. Geochemistry International 15, 66–69.

Raith, M. 1976: The Al-Fe(III)-epidote miscibility gap in a metamorphic profile through the Penninic series of the Tauern Window. Contributions to Mineralogy and Petrology 57, 99–117.

Riciputi, L.R., Valley, J.W. & McGregor, V.R. 1990: Conditions of Archean granulite metamorphism in the Godthab–Fiskenaesset region, southern West Greenland. Journal of Metamorphic Geology 8, 171–190.

Smith, G.M. & Dymek, R.F. 1983: A description and interpretation of the Proterozoic Kobbefjord Fault Zone, Godthåb district, West Greenland. Rapport Grønlands Geologiske Undersøgelse 112, 113–127.

Stergiou, A.C., Rentzeperis, P.J. & Sklavounos, S. 1987: Refinement of the crystal structure of a medium iron epidote. Zeitschrift für Kristallographie 178, 297–305.

Thomassen, B. & Krebs, J.D. 2001: Palaeogene gold- and silver-bearing epithermal veins at Amdrup Fjord, southern East Greenland. Rapport Danmarks og Grønlands Geologiske Undersøgelse 2001/133, 78 pp.

Wells, P. 1976: Late Archean metamorphism in the Buksefjorden region, Southwest Greenland. Contributions to Mineralogy and Petrology 56, 229–242.

Windley, B.F. & Garde, A.A. 2009: Arc-generated blocks with crustal sections in the North Atlantic craton of West Greenland: crustal growth in the Archean with modern analogues. Earth-Science Reviews 93 (1–2), 1–30.